LIMNOLOGY
and
OCEANOGRAPHY: METHODS

Limnol. Oceanogr.: Methods 8, 2010, 16–29

An assessment of the accuracy and precision of water quality parameters retrieved with the Matrix Inversion Method.

Glenn Campbell[1,2] *and Stuart R. Phinn*[1]*

[1]University of Queensland, Centre for Remote Sensing and Spatial Information Science, School of Geography, Planning and Environmental Management, St Lucia, Queensland 4072, Australia

[2]Australian Centre for Sustainable Catchments & Faculty of Engineering and Surveying, University of Southern Queensland, Toowoomba, Queensland 4350, Australia

Abstract

There is an increasing demand for quantitative inland water quality observations from satellites. One approach to estimate water quality constituent (chlorophyll and other pigments, total suspended material, and colored dissolved organic matter) concentrations from remote sensing radiance measured over inland waters is to apply a Matrix Inversion Method (MIM). Using the Hydrolight® radiative transfer model and typical water quality constituent concentrations from subtropical Wivenhoe Dam, Australia, this article demonstrates that significant improvements in the accuracy and precision of retrieved water quality constituent values can be obtained by using semianalytically estimated values for the proportionality factor that are calculated separately for each spectral band of the MERIS sensor. Furthermore, it shows that overdetermined systems of equations can be used to mitigate the effect of unknown and endemic sources of error in the remote sensing system. The residuals left after the inversion of the reflectance spectrum can also be used to assign a reliability measure to the retrievals of total suspended material (TSM) and colored dissolved organic matter (CDOM), but not for chlorophyll *a*. The results of this study may be used to improve algorithms for the remote sensing of water quality for freshwater impoundments.

The reflectance spectrum of water is a result of the cumulative interactions of light with the water itself and its associated water quality constituents, including chlorophyll and other pigments, total suspended material, and colored dissolved organic matter (CDOM). To retrieve the water quality constituent concentrations from satellite or airborne remotely sensed data or from field spectroradiometers, it is necessary to invert the reflectance spectrum. A semianalytical inversion approach relies on modeling the interaction of the photons with water components including water molecules and dissolved and dispersed substances. The approach is not totally analytical as it uses empiricism to parameterize several of the terms in the model (O'Reilly et al. 1998; Rijkeboer et al. 1997). The water quality constituent concentrations and the reflectance spectrum are linked through the three inherent optical properties (IOPs) of the water. These three properties have magnitudes that are independent of the geometric structure of the light field. The absorption coefficient a describes the chances of a photon being absorbed, the scattering coefficient b describes the chances of a photon being scattered, and the volume scattering function (VSF) $\beta(\theta)$ describes the probability of a scattered photon being scattered in a particular direction. Any successful semianalytic inversion approach needs to relate the reflectance to the IOPs and then the IOPs to the water quality constituent concentrations. This article describes how a reflectance model can be inverted to retrieve the water quality constituent concentrations and presents options for parameterizing the models and the effect of potential error sources on the water quality constituent retrieval accuracy.

Whereas there are a multitude of individual approaches to model inversion for water quality remote sensing, the majority fall within three general types: the look up table approach

*Corresponding author: E-mail: s.phinn@uq.edu.au

Acknowledgments

The authors would like to thank CSIRO for aid in the field work, laboratory work, and for assistance with Hydrolight software. In particular, we would like to thank Mr. Paul Daniel for his assistance in the field operations, Ms. Lesley Clementson for the laboratory measurements, and Dr. Arnold Dekker and Dr. Vittorio Brando for their valuable comments on the final manuscript. We would like to thank the European Space Agency for providing the MERIS FR image under the AO 595 agreement and SEQWater for the provision of historical water quality data.

which matches measured spectra to large number of previously calculated spectra (Keller 2001; Lee et al. 1999; Matarrese et al. 2004; Mobley et al. 2005); the neural network approach which uses a large set of training data to relate the measured spectra to the parameters used to create the training set (Baruah et al. 2001; Schaale et al. 1998; Schiller and Doerffer 1999; Su et al. 2006); and the inversion/optimization approach. The two former approaches have value, however, it is necessary to limit the scale of this article, and so, they are considered as outside the scope of this work.

In the inversion/optimization approach, a forward model is used to simulate the water reflectance spectra from a set of inherent optical properties and the set that gives the closest match is selected as the solution. The closest match is determined by evaluating a selected cost function, which will translate the differences between model and reference values in each band into a single value. Those approaches that directly invert the model to recover the water quality constituent values will be referred to as inversions. If the model is linear and the cost function is the sum of the squares of the residuals, then this reduces to the matrix inversion method (MIM). The optimization approach uses a forward model to calculate a reflectance spectrum from water quality constituent values and then uses a similarity measure to match it to the measured reflectance spectrum.

The MIM approach models the measured subsurface irradiance reflectance $R(0^-)$ as a function of the absorption and backscattering coefficients in each band and then solves the resultant system of linear equations. With increases in the number of bands in more recent satellite imaging instruments, there have been moves from using exact (same number of bands as unknowns) systems (Brando and Dekker 2003; Hoge and Lyon 1996; Hoge et al. 1999; Hoogenboom et al. 1998b; Lyon and Hoge 2006) to overdetermined (more bands than unknowns) systems (Boss and Roesler 2006; Hakvoort et al. 2002; Vos et al. 2003).

Once the system is overdetermined, the solution of the equation system cannot be exact because of errors in the measurement and model, so the MIM method uses the sum of the squared residuals to find the solution that minimizes this error. If an iterative approach is taken, then it is possible to extend weighted least squares to cover nonlinear problems where it has been shown that the residuals are smaller for the nonlinear model than for a comparable linear model (Vos et al. 2003). Like some of the spectral matching techniques, there is the risk that the nonlinear MIM will find a local minimum dependent on the starting point, rather than the absolute minimum (Keller 2001).There has been little work done on the effects of overdetermined systems except a finding that the MIM method was less accurate when using 15 or more bands (Vos et al. 2003) and that the need to convolve the IOPs with the response function of the sensor leads to a biased error especially for broad bands (Keller 2001). Work by Lee and Carder (2002) showed that for deep water, there was no difference in the performance of 5 nm, 10 nm, 20 nm contiguous bands and the MERIS band set. They found a difference between the contiguous bands and MERIS for shallow waters. Although they were using inversion optimization, it is likely that a similar result will be obtained with MIM.

Few publications compare the performance of inversion methods. Keller (2001) found that the standard deviation of the results of MIM was lower than the curve-fitting result, but the result was closer and more consistent for chlorophyll *a* (Chl *a*) with curve fitting. Unfortunately, the work limited itself to a single water quality constituent concentration. An International Ocean-Color Coordinating Group (IOCCG) report (Lee 2006) compared the performance of eight algorithms designed to retrieve the IOPs, rather than the water quality constituent concentrations. Each algorithm was applied to large synthetic and in situ data sets. There was a greater variation in performance across the synthetic data set, but this may only reflect the deviation of the bio-optical model behind each algorithm, from that of the bio-optical model used to prepare the synthetic data set. There was little variation in the performance of the algorithms on the in situ data set. A main conclusion from the IOCCG report was that a better quantification of uncertainties in derived products through an in-depth analysis of error sources and their propagation is required (Lee 2006).

The performance of an inversion method can be measured by the difference between the estimated value and a reference value, its accuracy, and a measure of the minimum detectable difference in a measured or estimated parameter, its precision. The accuracy and precision of the MIM for estimating water quality from reflectance data depends on the width, position, and inherent noise in the spectral bands of the sensor being employed, as well as the radiometric corrections applied to images to calculate the subsurface reflectance. Accuracy and precision can be affected by other elements of the algorithm design; for example, in overdetermined systems the reliance of the solution on any one band can adjusted by differentially weighting the band equations. However, there are unquantifiable errors associated with spatial and temporal patterns in the dynamic nature of the aquatic environment, which make it difficult to establish the retrieval accuracy for the water quality constituent concentrations. Fortunately the subsurface reflectance can be modeled with Hydrolight 4.2®, a numerical model that solves the radiative transfer equation to produce radiance distributions and derived quantities for natural waters (Mobley and Sundman 2001). Comparisons between the original and retrieved water quality constituent values make it possible to quantify the effect of each element of the algorithm or the effect of known error sources.

The aim of this work was to establish the optimum algorithm design to implement water quality monitoring for tropical and subtropical inland waters using the European Space Agency's MERIS sensor or similar future sensors.

Materials and procedures

Reflectance model—The most common semianalytical model for in-water reflectance was developed by Gordon et al. (1975) using the optical depth τ as the independent variable.

$$R(\tau,-) = \sum_{n=0}^{N} r_n(\tau) X^n \;,\; X = \frac{\omega_0 B}{(1-\omega_0 F)} \;,\; \tau = \int_0^z c(z)dz \qquad (1)$$

B and *F* are the backscattering and forward scattering probabilities and ω_0 is the ratio between the total scattering coefficient *b* and the total attenuation coefficient *c*. The constants in the polynomial equation $r_n(\tau)$ are dependent on the illumination conditions. As $B = 1 - F$ the equation for the subsurface irradiance reflectance can be represented in the more common form.

$$R(0^-) = \sum_{n=0}^{n=3} f_n(0)\left(\frac{b_b}{a+b_b}\right)^n \qquad (2)$$

Whilst the scattering and absorption coefficients are spectral in nature, dependence on wavelength has been omitted for clarity. For convenience ω_b will be defined as

$$\omega_b = \frac{b_b}{a+b_b} \qquad (3)$$

Proportionality factor (f)—There are two ways to account for the nonlinear nature of the reflectance and ω_b relationship. Nonlinear systems of equations can still be solved using a least-squares approach, but this involves using an iterative solution that comes at a computational cost. Alternatively the model can be linearized by truncating the higher order terms and a single proportionality factor (*f*). It was shown that the error from leaving out the second and third order terms is approximately $\omega_b/(1+\omega_b)$ (Gordon et al. 1988), which equates to 20% for the simulation sets used in this paper.

Aas (1987) showed that the proportionality factor was related to shape factor for scattering in the upward (r_u) and downward (r_d) direction. If the simplifications, $r_u = r_d = 1$ (Dekker et al. 1997), a completely diffuse upwelling light field, and a downwelling light completely dominated by μ_0 (the cosine of sun zenith) are made (Walker 1994 as cited in Phinn and Dekker 2005), the proportionality factor can be approximated by

$$f = \frac{1}{1+2\mu_0} \qquad (4)$$

However r_d of 1.3–10 and r_u of 1.8–20 have been modeled for the development of a *Platymonas* algal bloom in Case I waters (Stavn and Weidemann 1989). The shape factors rose slowly as the Chl *a* plus phaeopigments concentration increased until it reached 0.1 mg m^{-3} then the shape factors increased exponentially. The use of a constant proportionality factor may have a significant effect on the model accuracy.

Alternatively, the attempt to calculate *f* analytically can be abandoned and a semianalytical approach used. In this case, a portion of the IOP dependence can be transferred to the proportionality factor *f*. In this approach, *f* becomes the ratio of reflectance and $\omega_{b,}$ and it should have a shape that can be modeled by a polynomial. The relationship can be used to estimate *f* for a forward model as the value of ω_b will be known, but it is of no use in inverting the measured reflectance spectra as ω_b is unknown. Therefore, we use the approach by Brando and Dekker (2003) to calculate *f* for a backward model.

It has already been shown that for the first order approximation reflectance is a function of ω_b. If this is the case then a plot of *f* against reflectance should have a very similar shape to the previous relationship. An example of the relationship is plotted in Fig. 1 where the Hydrolight-modeled spectra were convolved with the MERIS band response functions.

Brando and Dekker (2003) ran a similar series of 1331 Hydrolight simulations with IOPs that varied within the range of measured values for Moreton Bay, Australia. From the result, they were able to calculate a quadratic equation for *f* in terms of $R(0^-)$ which had an R^2 of 0.999 and showed a variation in *f* from 0.339 to 0.472.

The shape of the light field will be dependent on the scattering and absorption IOPs of the water and the water quality constituents in question as well as the illumination properties. As the IOPs are not spectrally invariant, it is logical to presume that the shape of the light field for each wavelength will be different. The parameters of the polynomial fit for *f* in terms of $R(0^-)$ will reflect the shape of the light field and hence the relationship between *f* and $R(0^-)$ is not spectrally invariant either as illustrated in Fig. 1 for the MERIS bands.

Water quality constituent inherent optical property models—The inherent optical properties of water are modeled as a sum of the inherent optical properties of pure water and the water quality constituents suspended and dissolved in it.

Absorption—A four part absorption model was used.

$$a(\lambda) = a_w(\lambda) + a_{CDOM}(\lambda) + a_{TSM}(\lambda) + a_\phi(\lambda) \qquad (5)$$

The subscripts *w* and ϕ refer to water and Chl *a*, respectively. The values for $a_w(\lambda)$ were obtained from Pope and Fry (1997) and Smith and Baker (1981). The absorption due to the water quality constituents is proportional to the concentration of the constituent. This is normally represented by the use of a specific absorption coefficient.

$$a_i(\lambda) = C_i a_i^*(\lambda) \qquad (6)$$

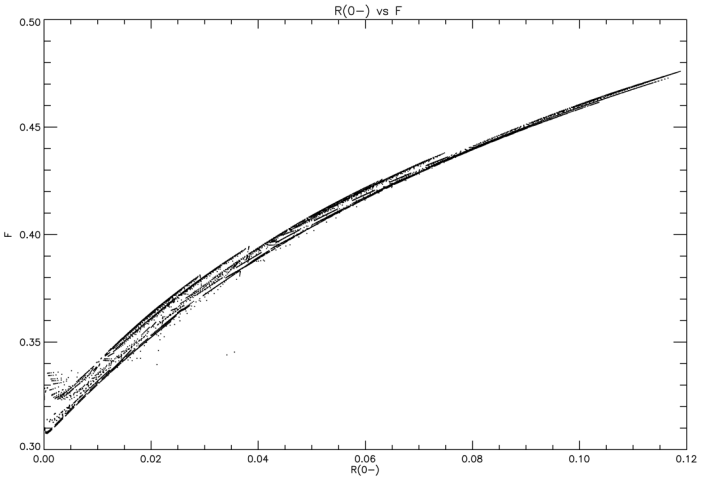

Fig. 1. Plot of *f* as a function of $R(0^-)$ modeled with Hydrolight. The reflectance was modeled between 400 nm and 800 nm using a solar zenith angle θ_0 = 0°, a clear sky and an average IOP set for Wivenhoe Dam. The resulting spectra were convolved with the MERIS band response functions.

The specific absorption spectra were sourced from the field measurements of Wivenhoe Dam, Australia in July 2007 and are shown in Fig. 2.

Scattering and backscattering—The scattering coefficient *b* is combined with the volume scattering function (VSF) β(θ) to calculate the probability of a photon being scattered in a direction greater than 90° from its initial direction of travel. This is referred to as the backscattering.

A three-part backscattering model was used.

$$b_b(\lambda) = b_{bw}(\lambda) + b_{bTSM}(\lambda) + b_{b\phi}(\lambda) \tag{7}$$

The scattering coefficient for pure water was obtained from Morel (1974) and a ratio of b_w:b_{bw} of 0.5 was used. The backscattering of tripton and phytoplankton proportional to the concentration of the constituent and were obtained from the field measurements of Wivenhoe Dam in July 2007 and are shown in Fig.2.

Matrix inversion method—After omitting the spectral dependence for the proportionality factor, the linearized version of the Gordon et al. (1975) model is:

$$R(\lambda_i) = f(\omega_b, \mu_0)\frac{b_b(\lambda_i)}{a(\lambda_i) + b_b(\lambda_i)} \tag{8}$$

For a given wavelength, substituting Eqs. 5 to 7 and into 8 and rearranging (Hoge and Lyon 1996) gives equation 9 (shown at the bottom of the page).

This can be represented in a matrix form for all wavelengths of the spectra as equation 10 (shown at the bottom of the page).

Or

$$y = Ax \tag{11}$$

where A is a 3 × N dimension matrix with N being the number of bands used by the inversion.

The standard solution for this problem is

$$x = [A^TA]^{-1}A^Ty \tag{12}$$

It has been asserted but not demonstrated that application of the weighted least-squares method significantly improves the accuracy of the results (Hakvoort et al. 2002).

The weight matrix is a square (N × N) diagonal matrix (W) where W_{ii} = relative weight of band *i*. The weights are chosen to give greater influence to those bands that are deemed to be more reliable.

The solution then becomes

$$x = [A^TWA]^{-1}A^TWy \tag{13}$$

Weighting schemes—The interplay between the band weights and the performance of the MIM is too complex to be characterized analytically; rather a number of suppositions will be tested to see which returns the most accurate and precise results.

$$\frac{R}{f(\omega_b,\mu_0)} = \frac{b_{bw} + TSM \cdot b_{bTSM} + CHL \cdot b_{b\phi}}{a_w + CDOM \cdot a_{CDOM} + TSM \cdot a_{TSM} + CHL \cdot a_\phi + b_{bw} + TSM \cdot b_{bTSM} + CHL \cdot b_{b\phi}} \tag{9}$$

$$\begin{bmatrix} a_w(\lambda_1)\frac{R(\lambda_1)}{f} - b_{bw}(\lambda_1)\left(1 - \frac{R(\lambda_1)}{f}\right) \\ \vdots \\ a_w(\lambda_n)\frac{R(\lambda_n)}{f} - b_{bw}(\lambda_n)\left(1 - \frac{R(\lambda_n)}{f}\right) \end{bmatrix} = \begin{bmatrix} a^*_\phi(\lambda_1)\frac{R(\lambda_1)}{f} - b^*_{b\phi}(\lambda_1)\left(1 - \frac{R(\lambda_1)}{f}\right) & \cdots \\ \vdots & \\ a^*_\phi(\lambda_1)\frac{R(\lambda_1)}{f} - b^*_{b\phi}(\lambda_1)\left(1 - \frac{R(\lambda_1)}{f}\right) & \cdots \end{bmatrix} \begin{bmatrix} CHL \\ TSM \\ CDOM \end{bmatrix} \tag{10}$$

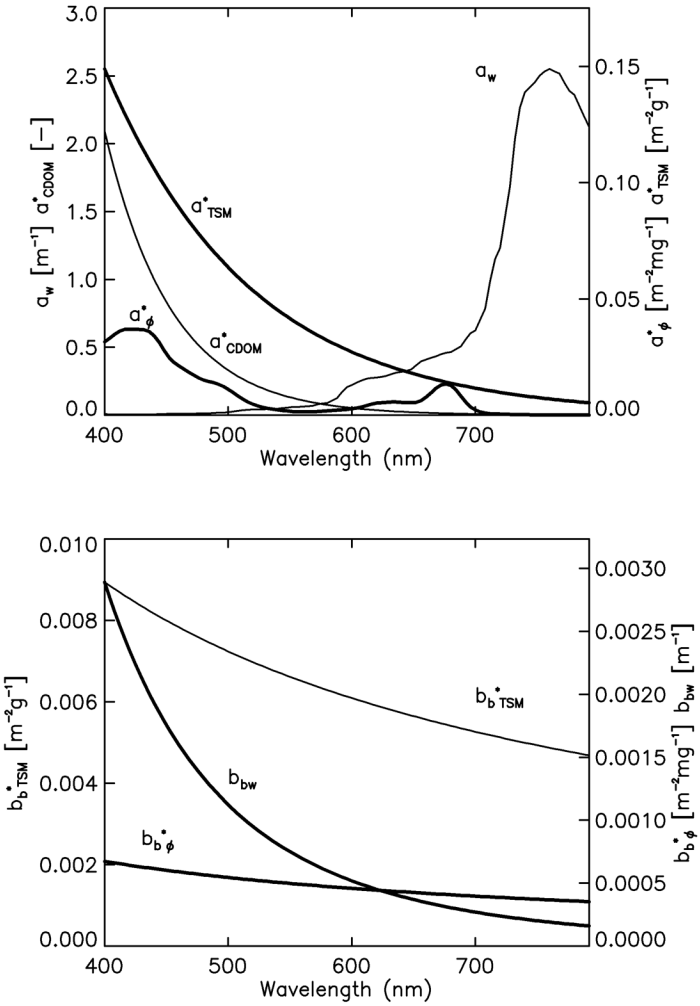

Fig. 2. Average SIOPs for Wivenhoe Dam. The upper graph shows the spectral absorption of water (*w*) and the specific absorption spectra of Chl *a* (ϕ), total suspended material (*TSM*), and colored dissolved organic matter (CDOM). The lower shows the spectral backscattering of water (*w*) and the specific backscattering spectra of Chl *a* (ϕ) and total suspended material (TSM).

The first family of weighting schemes represent the conventional approach where all bands are given equal weighting (ALL and NO_IR) or where exactly determined systems of equations of a priori selected bands have been used (3BANDS). In this case, the three bands selected were as close as possible to those used by Brando and Dekker (2003), two centered at 490 and 670 nm and one in the 700–740 nm range.

The next family of weighting schemes assumes that there is a uniform noise in reflectance (Hakvoort et al. 2002) meaning that those bands with a high value of reflectance should have a higher signal to noise ratio and thus will be more reliable (HAK and REF). As the shape of the reflectance spectrum changes with the concentrations of the water quality constituent, weights representing low, mid, and high water quality constituent concentrations were selected.

Giardino et al. (2007) and Hoogenboom et al. (1998a) make the argument that bands which exhibit the greatest change in reflectance when an increase in a water quality constituent concentration occurs should be of greater use in determining the concentration. The change in reflectance with a change in a water quality constituent concentration is measured by the first derivative of the spectra with respect to the water quality constituent concentration (DER). Using the Hydrolight simulations, the derivatives were calculated and used to create the next family of weighting schemes.

The last family were derived empirically (RAN). The weights were allowed to vary randomly and those that performed the best were retained and the commonalities of the best performed schemes were combined.

Study site and field measurements—Lake Wivenhoe is located in the upper Brisbane River in South East Queensland, Australia. Risk assessments characterize the overall water quality rating as moderate and the cyanobacterial rating as poor (Orr and Schneider 2006).

During July 2007, the IOPs of the storage were measured at nine stations between the dam wall and the Esk offtake tower (Fig. 3). Water samples were taken from the near surface water and kept cool for later laboratory measurement of total suspended material (TSM), Chl *a* (CHL) concentration, and CDOM concentration. The Chl *a* concentration was measured by filtering water samples through a 47 mm diameter GF/F glass-fiber filter (pore size of 0.7 µm). The samples were then extracted from the filters over 15–18 h in an acetone solution before analysis by HPLC following a modified version of the Van Heukelem and Thomas (2001) method. The TSM was measured by filtering water samples through preweighed 47 mm diameter GF/F filters that had been prepared according to the MERIS calibration protocols. The filters were weighed after they were oven dried at 60°C to constant weight. The spectral absorption for TSM and Chl *a* were measured by filtering the water samples through a 25 mm diameter GF/F glass-fiber filter (pore size of 0.7 µm), and the spectral absorption was measured with a GBC 916 UV/VIS dual beam spectrophotometer with integrating sphere (Clementson et al. 2001). The pigmented material was extracted (Kishino et al. 1985) and then the spectral absorption was remeasured. The phytoplankton spectral absorption was obtained by taking the difference between the two spectra. The CDOM samples were filtered through a 0.22-µm polycarbonate filter using an all glass filtering unit. The filtrate had its absorbance measured using a 10 cm path length quartz cell in a GBC 916 UV/VIS spectrophotometer, with Milli-Q water (Millipore) as a reference.

At each station, the water was pumped for a minimum of 10 min from approximately 0.5 m below the surface, settled to remove air bubbles, and then gravity fed successively through a conductivity-temperature sensor and a WET Labs absorption and attenuation meter (ac-9) (WET Labs 2005), and finally emptied into a black plastic container. In the container, the

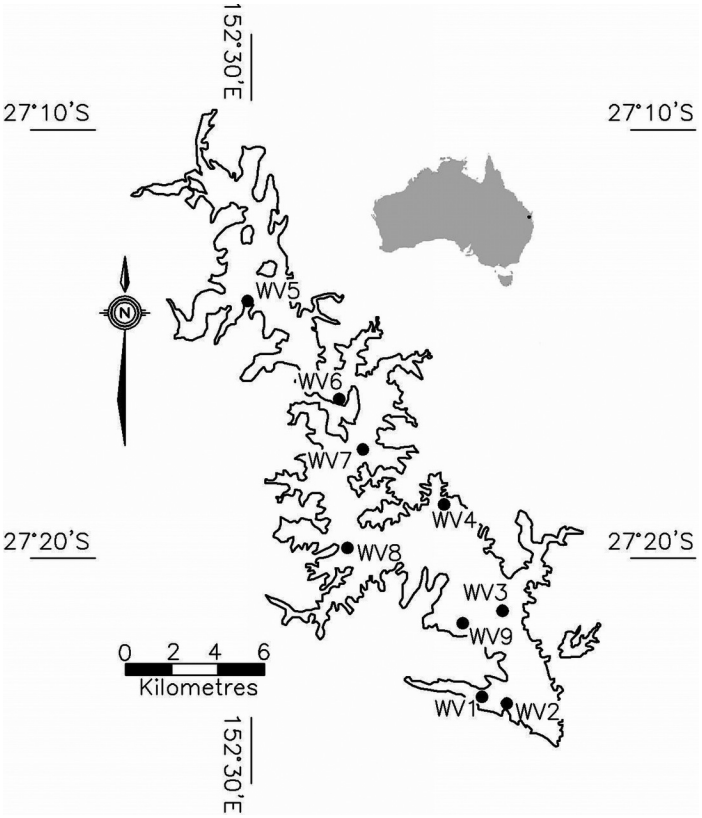

Fig. 3. Location of the SIOP sample sites for the July 2007 fieldwork activities on Wivenhoe Dam, Australia.

Table 1. Water quality constituent concentrations and modeling parameters used in simulation of reflectance spectra.

Water quality constituent	Concentration
Chlorophyll *a* (μg L^{-1})	0,2,4,6,8,10,12,14,16,18,20
TSM (mg L^{-1})	0,2,4,6,8,10,12,14,16,18,20
CDOM (a_{CDOM} @440 nm [m^{-1}])	0,0.1,0.2,0.3,0.4,0.5,0.6,0.7,0.8
Sun zenith angle (°)	0,9.5,19.1,29.0,36.9,43.5,49.5,54.9,61.1

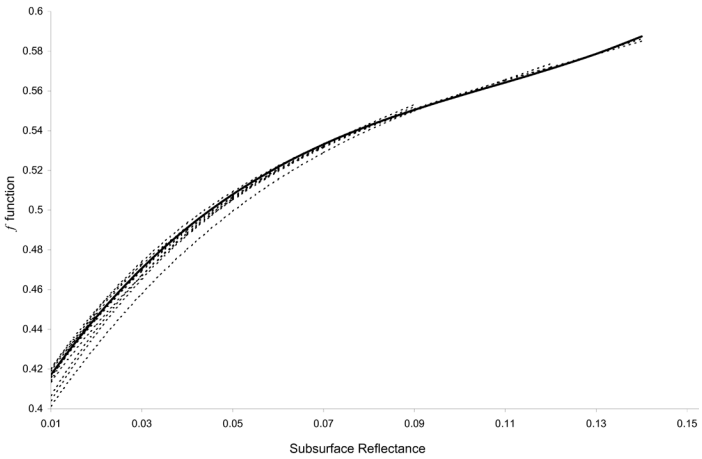

Fig. 4. Plot of *f* as a cubic function of $R(0^-)$ modeled within each band MERIS spectral band with Hydrolight. The reflectance was modeled between 400 nm and 800 nm using θ_0 = 54.9°, a clear sky and an average IOP set for Wivenhoe Dam. The functions have been cut to show only the valid range for $R(0^-)$. The function calculated for the set as a whole is shown in bold, and the separate band functions are shown dotted.

scattering properties were measured using a HydroScat-6 (Maffione and Dana 1997). A separate measurement of the backscattering of phytoplankton cells was not feasible; the assumption was made that 1 μg L^{-1} of CHL was approximately equal to 0.07 mgl^{-1} TSM (Buiteveld et al. 1994).

Hydrolight simulations—Based on monitoring data over the last 5 yr supplied by SEQWater, 1089 Hydrolight simulations were run for each sun position at the water quality constituent concentration values shown in Table 1. As SEQWater does not regularly measure CDOM absorption at 440 nm values the range was estimated based on field measurements.

The simulations used average IOP values from the 2007 site visit at 1 nm steps between 401–799 nm using a clear sky with the default Hydrolight atmosphere, an infinite depth and a wind speed of 1 m/s. To model the effect of the sun position, nine simulation sets were run for clear skies with the sun zenith angle varying from 0° to 61.1°. The angles were selected so that their cosines were well distributed. The simulated spectra were then convolved with the first twelve MERIS bands (412.5 nm, 442.5 nm, 490 nm, 510 nm, 560 nm, 620 nm, 665 nm, 681.25 nm, 708.75 nm, 753.75 nm, 760.625 nm and 778.75 nm).

Parameterizing the models—For each sun position, a quadratic and a cubic function were used to model *f* as a function of subsurface reflectance. The coefficients were then plotted against the secant of the in-water sun angle $[1/\cos(\theta_w)]$ to obtain functions to allow the generation of coefficients for any sun position within this range.

To examine the wavelength effect on the proportionality factor a cubic function was fitted to a representative Hydrolight run (θ_0 = 54.9°), and the residuals were separated by wavelength. The mean residual of the fit for all bands was zero as expected but the individual bands showed distributions that peaked at positive or negative values. The simulation sets were then used to recalculate the *f* and $R(0^-)$ relationship using reflectances from single bands. Fig. 4 shows the resulting functions. Each function has been cut to only show the range of $R(0^-)$ for that band.

To investigate the effect of splitting the *f* function into band specific functions the difference between the Hydrolight calculated *f* and the calculated *f* from the single function and the band specific function were compared. Fig. 5 shows plots of the residuals using the single function and the band split function. It is clear that there is a considerable improvement in the quadratic function but less so in the cubic function. Further investigation showed that only 59.8% of the residuals are reduced and the rest are increased. However the median value of reduction is 45% larger than the median value of

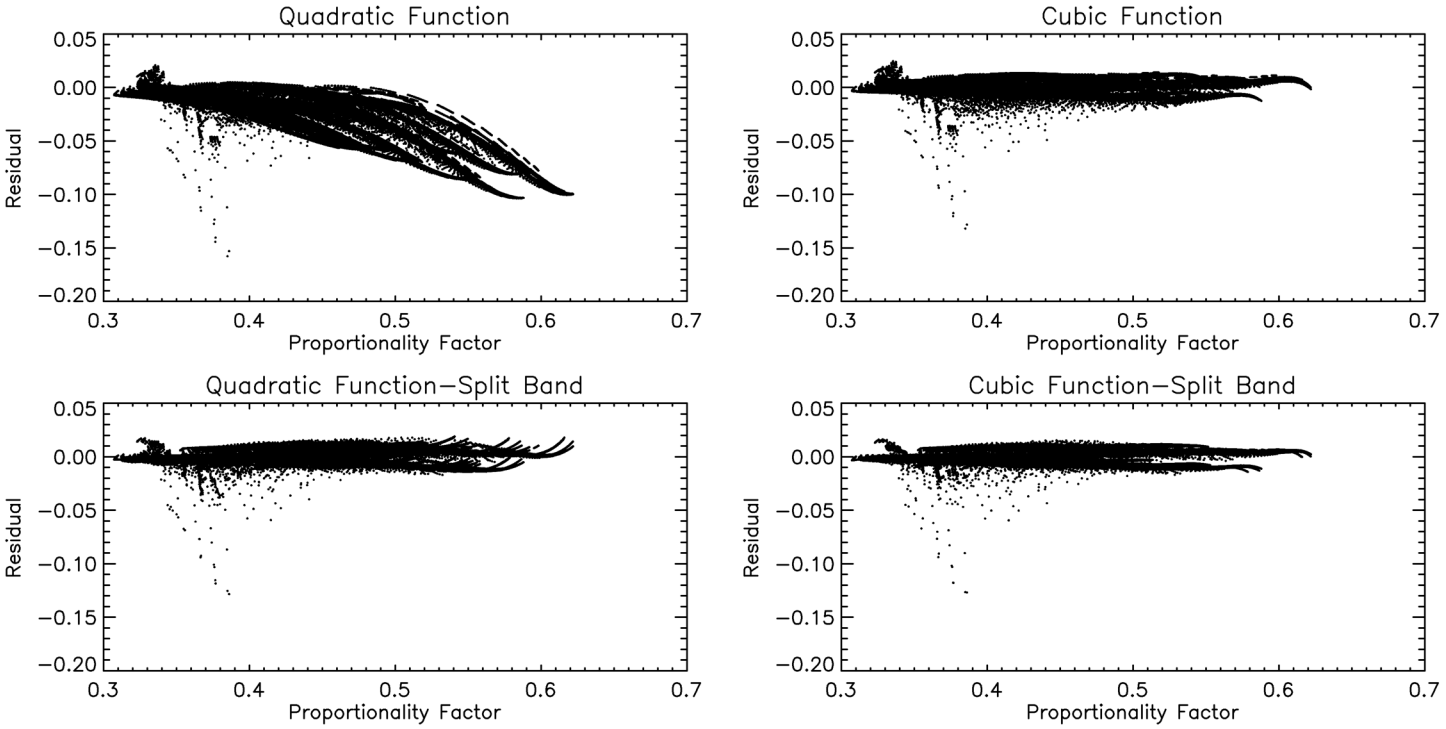

Fig. 5. Plots of the residuals for all sun positions using the single function and the band split function for the quadratic and cubic inverse model.

increase. In short, there are more improved residuals, and in general, the amount of improvement is greater.

Simulation of noise—The bio-optical models described above relate the subsurface reflectance to the absorption and backscattering of the water and water quality constituents. As a remote sensor measures the top of atmosphere radiance, the effect of the atmosphere and the air-water interface must be eliminated before the subsurface reflectance spectra can be used. In addition the inversions rely on having accurate specific absorption and backscattering spectra. Any measurement errors, approximations, or assumptions made in this process will introduce error into the retrieved water quality constituent concentrations. The ability of a weighting scheme to alleviate the effect of these errors will be a useful measure of its efficacy.

To simulate the effect of three broad types of error, the following distortions were made to the simulated spectra or the SIOPs.

Environmental noise errors—Some errors act separately in each band meaning the reflectance spectra is distorted in shape as well as scale. Some of the sources of this variation are

- A single value of the ratio of upwelling irradiance to upwelling radiance (Q) is used in the air-water interface correction of De Haan and Kokke (1996) but the Hydrolight simulations show this value varies by approximately 4.6% (range 4.52–4.96).
- The average error between the fitted curve and the raw data for the proportionality factor f was 1%.
- The environmental noise-equivalent radiance difference $[NE\Delta R(0^-)_E]$ is the standard deviation of the subsurface reflectance in each band over a homogeneous area of optically deep water (Brando and Dekker 2003). Using a MERIS full resolution image acquired on the 2 July 2007 corrected using c-WOMBAT-c (Brando and Dekker 2003) $[NE\Delta R(0^-)_E]$ was estimated to be a constant 0.1% in all bands.

For eight noise levels between 0% and 7%, these errors were imitated by adding in a simulated spectrum, a normally distributed, pseudo-random number with a mean of zero and a standard deviation of one that was scaled to the particular noise level to each band. An offset representing the $NE\Delta R(0^-)_E]$ was then applied. As each band had a different scale factor applied to it, the effect was to distort the shape as well as the scale of the spectra. The inversion was run on the 9801 simulated spectra with 50 applications of the noise. The inversion algorithm was applied and the mean of the 50 mean errors was calculated for each water quality constituent value at each noise level.

Atmospheric correction errors—The errors associated with the atmospheric correction distort the magnitude and shape of the spectrum as before, but in this case, the amount of the error in each band will be correlated. In broad terms, the error in magnitude will occur when an incorrect estimate has been made of the visibility and the shape error will occur from making a poor estimation of the aerosol types or their mixing ratio. The spectral dependence of the path radiance conforms to a power law so the spectra were modified by single multiplicative scale

factor (varying from unity by 0% to 20%, normally distributed) as well as a value for the power slope (varying from unity by 0% to 10%). The inversion was run as described in the previous section.

SIOP measurement errors—The MIM method requires that the spectra for a^* and b^*_b be calculated from field measurement of the total absorption and backscattering for each constituent and the water quality constituent concentration. Measurement errors in the water quality constituent concentration, due to the limitations of the laboratory techniques, will result in a consistent scale error across all bands as the water quality constituent concentration is used as a divisor for each band when the SIOP is calculated. In addition, the measurement of absorption and backscattering for each constituent will have a shape error associated with it due to random errors in their measurement because the errors are not necessarily consistent across the spectrum. For the phytoplankton absorption, the shape change was modeled in the same way as the signal shape error. The other water quality constituents' absorption and the backscattering calculations involve fitting a function with slope and scale parameters to the raw observation so their errors were modeled using a variation of spectral slope in the same way as the atmospheric correction error. After considering the variation in SIOPs measured during the July 2007 site visit, the phytoplankton SIOP scale error bounds were set to 0% and 20%, and the noise applied to the slope was set at half the value for the scale. The absorption and scattering of pure water was not varied. The inversion was run as described in the previous section.

Assessment and discussion

The accuracy and precision of the inversion methods were established by inverting the spectra simulated with the Hydrolight code. The accuracy of any given spectrum inversion was evaluated by the absolute value of the difference between the retrieved water quality constituent value and the value used to simulate the spectra. The average value over all the spectra in all nine simulations was considered the accuracy of that water quality constituent for that inversion routine. The precision was measured by the standard deviation of all absolute values of the differences between the retrieved water quality constituent values and the values used to simulate the spectra. These accuracies and precisions will represent the baseline or best possible values.

The baseline values for the MIM for Wivenhoe Dam water are reported in Table 2 for both the quadratic and cubic formulations of the *f* value. It is clear that the cubic function provides the most accurate and precise results for all of the weighting schemes. Table 3 shows the baseline values for the MIM when the *f* function is made band specific. There is substantial improvement for the quadratic function across all three water quality constituent types. There is considerable improvement in the Chl *a* retrieval accuracy when the band specific cubic function is used and a marginal improvement in the other water quality constituents. The band specific cubic *f* function will be used in the estimation of effects of the other noise sources.

Accuracy and precision values after the addition of environmental noise—Before introducing simulated error from the other sources the offset representing the $NE\Delta R(0^-)_E$ was applied. Fig. 6 compares the average error before the application of the noise against the average error after the noise is applied. The most obvious feature is that the standard three band approach has performed very poorly with the addition of the $NE\Delta R(0^-)_E$. However, there has also been a change in the best performed weighting schemes.

Previous work (Campbell and Phinn 2008) has shown differences in the behavior of the weighting schemes with respect to the introduced noise. This behavior was ascribed to the weighting schemes themselves but it now appears to be an artifact of the poor fitting of the *f* function to the individual bands. Using the band specific *f* function ensures that nearly all the weighting schemes behave in essentially the same manner when environmental noise is added. Fig. 7 shows examples of the error-noise relationship. It can be seen that the three band approach has a large variability in the water quality constituent retrieval. For all three water quality constituents, the MER_ALL weighting scheme is least affected by the increase in the environmental noise but its overall utility is limited by its response to the $NE\Delta R(0^-)_E$ offset.

If we exclude the three band weighting scheme the addition of the $NE\Delta R(0^-)_E$ offset increased the standard deviation of the absolute error by between 10–30 times for Chl *a*, 1.2–16 times for TSM, and 1.9–2.6 times for CDOM. In the case of Chl *a* and CDOM, the addition of the other noise sources had a negligible effect on the retrieval precision. However, in the case of the TSM retrieval the precision varies in proportion to the accuracy.

Accuracy and precision values after the addition of atmospheric noise—Sample plots of the atmospheric noise-error relationship are shown in Fig. 8. For all intents and purposes, the water quality constituent error values follow a linear trend with the increase in atmospheric noise. The water quality constituent retrieval precision varies in proportion to the accuracy.

Accuracy and precision values after the addition of SIOP noise—Sample plots of the SIOP noise-error relationship are shown in Fig. 9. Like the effect of atmospheric noise, the error increase is linear, for the most part, with the addition of noise in the SIOP set. It is clear that none of the weighting schemes are superior in relation to the retrieval of TSM, but once again, the three band scheme performance is degraded more sharply by the addition of SIOP noise. The water quality constituent retrieval precision varies in proportion to the accuracy.

The preceding results were used to rank the weighting schemes to identify those that give the best all-round performance for the three water quality constituent types and the three sources of noise. The six best performed weighting schemes are shown in Fig. 10. With the exception of the three-band

Table 2. The means of the means of the absolute values of error for inversions at nine different sun angles using a single parameter function for all bands.

	Quadratic						Cubic					
	Chl (μg L^{-1})		TSM (mg L^{-1})		CDOM(m^{-1})		Chl (μg L^{-1})		TSM (mg L^{-1})		CDOM(m^{-1})	
Weight scheme	Av	SD	Av	SD	Av	SD	Av	SD	Av	SD	Av	SD
MER_ALL	2.49	1.88	0.98	0.8	0.03	0.03	0.23*	0.16	0.17	0.14	0.02	0.02
MER_NO_IR	1.99	1.13	1.64	1.42	0.05	0.04	0.22	0.15	0.17	0.16	0.02*	0.02
MER_3BANDS	2.94	1.55	1.09	0.96	0.09	0.07	0.3	0.2	0.15	0.15	0.02	0.02
MER_DER1	2.13	1.33	1.47	1.24	0.08	0.05	0.23*	0.18	0.17	0.15	0.02†	0.02
MER_DER2	1.69	1.19	1.36	1.14	0.08	0.05	0.23	0.17	0.17	0.15	0.02§	0.02
MER_DER3	1.47	0.88	1.26	1.05	0.1	0.05	0.22	0.16	0.17	0.15	0.02§	0.02
MER_DER4	8.35	4.61	3.57	2.98	0.06	0.05	0.43	0.38	0.29	0.27	0.02	0.02
MER_DER5	1.64	1.14	1.38	1.18	0.08	0.05	0.22	0.17	0.17	0.15	0.02‡	0.02
MER_DER6	1.53	1.08	1.35*	1.16	0.08	0.05	0.21	0.17	0.17	0.15	0.02‡	0.02
MER_HAK	1.42	0.86	1.27	1.07	0.1	0.05	0.22	0.16	0.17	0.15	0.02	0.02
MER_REF1	4.63	1.83	1.83	1.56	0.11	0.07	0.28	0.23	0.19	0.17	0.02	0.02
MER_REF2	1.47	1.03	1.37	1.15	0.09	0.05	0.22	0.17	0.17	0.15	0.02	0.02
MER_RAN1	0.54	0.39	1.49	1.29	0.05	0.05	0.25	0.14	0.16	0.16	0.02†	0.02
MER_RAN2	0.84	0.69	1.36	1.18	0.05	0.04	0.27	0.15	0.16*	0.15	0.02*	0.02
MER_RAN3	1.02	0.75	1.18	1.06	0.04	0.03	0.25	0.16	0.16	0.15	0.02	0.02
MER_RAN4	1.18	0.75	1.19	1.04	0.05	0.03	0.2	0.15	0.16*	0.15	0.02	0.02
MER_RAN5	1.6	1.16	1.26	1.07	0.03	0.03	0.23	0.16	0.16	0.15	0.02	0.02
MER_RAN6	2.5	1.76	1.00	0.81	0.13	0.07	0.26	0.17	0.17	0.14	0.02	0.02
MER_RAN7	6.42	4.13	1.03	0.78	0.05	0.04	0.37	0.26	0.17	0.14	0.02	0.02
MER_RAN8	12.19	7.68	1.35*	0.95	0.14	0.09	0.64	0.45	0.19	0.15	0.02	0.02

*, †, ‡, or § denotes the difference is not significant at 95% for pairwise comparisons.

Table 3. The means of the means of the absolute values of the error for inversions at nine different sun angles using separate parameter functions for each band.

	Quadratic						Cubic					
	Chl (μg L^{-1})		TSM (mg L^{-1})		CDOM(m^{-1})		Chl (μg L^{-1})		TSM (mg L^{-1})		CDOM(m^{-1})	
Weight scheme	Av	SD	Av	SD	Av	SD	Av	SD	Av	SD	Av	SD
MER_ALL	0.21	0.18	0.15	0.15	0.01	0.01	0.1	0.09	0.14	0.14	0.01	0.01
MER_NO_IR	0.15	0.15	0.16	0.18	0.01	0.01	0.08*	0.09	0.16	0.16	0.01	0.01
MER_3BANDS	0.22	0.2	0.15	0.15	0.02	0.02	0.16	0.13	0.14	0.14	0.02	0.02
MER_DER1	0.19	0.17	0.16	0.17	0.02	0.01	0.1	0.1	0.16	0.16	0.02	0.01
MER_DER2	0.19	0.17	0.16	0.17	0.02	0.01	0.1	0.1	0.15*	0.16	0.02	0.01
MER_DER3	0.19	0.16	0.15	0.16	0.02	0.02	0.08*	0.09	0.15	0.15	0.02	0.02
MER_DER4	0.41	0.43	0.27	0.33	0.01	0.01	0.34	0.34	0.26	0.28	0.01	0.01
MER_DER5	0.18	0.16	0.16	0.17	0.02	0.01	0.09	0.09	0.15	0.15	0.02	0.01
MER_DER6	0.18	0.16	0.15	0.17	0.02	0.01	0.09	0.09	0.15	0.15	0.02	0.01
MER_HAK	0.19	0.16	0.15	0.16	0.02	0.02	0.08	0.09	0.15	0.15	0.02	0.02
MER_REF1	0.24	0.21	0.18	0.19	0.02	0.02	0.18	0.15	0.17	0.18	0.02	0.02
MER_REF2	0.19	0.16	0.16	0.17	0.02	0.01	0.09	0.09	0.15*	0.16	0.02	0.01
MER_RAN1	0.13	0.14	0.15	0.17	0.01	0.01	0.07	0.07	0.15	0.15	0.01	0.01
MER_RAN2	0.14	0.15	0.15	0.16	0.01	0.01	0.08	0.08	0.15	0.15	0.01	0.01
MER_RAN3	0.15	0.15	0.15	0.16	0.01	0.01	0.07	0.07	0.14	0.14	0.01	0.01
MER_RAN4	0.16	0.15	0.15	0.16	0.01	0.01	0.08	0.08	0.15	0.15	0.01	0.01
MER_RAN5	0.17	0.16	0.15	0.16	0.01	0.01	0.1	0.09	0.15	0.15	0.01	0.01
MER_RAN6	0.22	0.19	0.15	0.15	0.02	0.02	0.1	0.1	0.15	0.15	0.02	0.02
MER_RAN7	0.34	0.31	0.15	0.15	0.01	0.01	0.27	0.22	0.15	0.15	0.01	0.01
MER_RAN8	0.62	0.59	0.17	0.17	0.01	0.01	0.49	0.45	0.16	0.16	0.01	0.01

* denotes the difference is not significant at 95%.

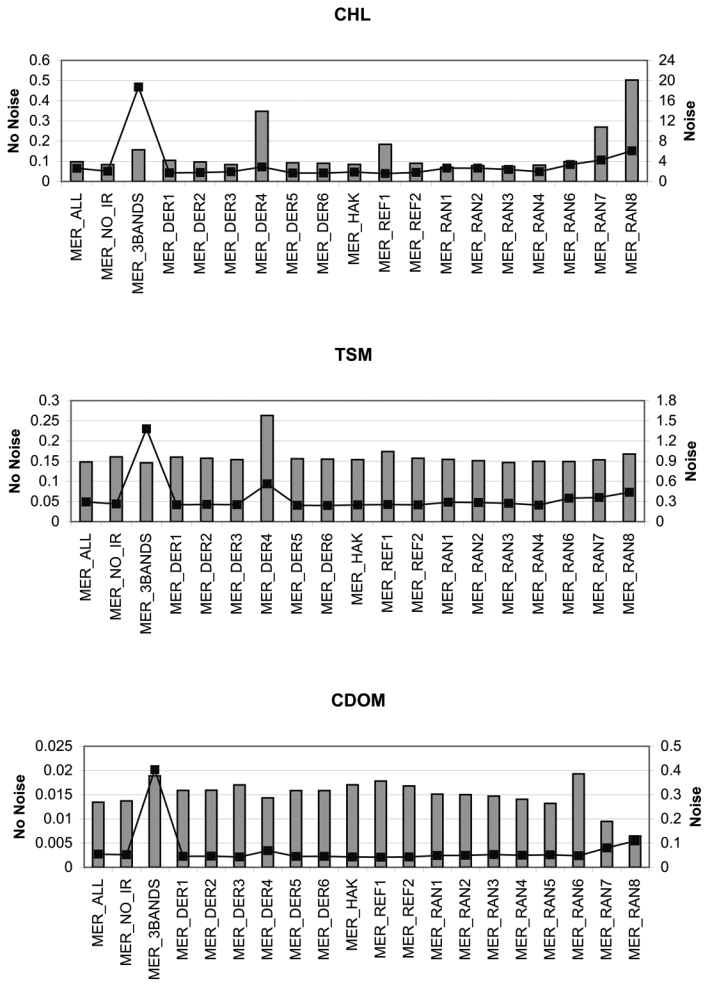

Fig. 6. Plots comparing the mean retrieval accuracy for Chl *a*, TSM, and CDOM with and without added noise. The retrieval was done using the band specific cubic *f* function. The bars are the noise-free averages, and the line is the average after addition of a NEΔ $R(0^-)$ of 0.001.

approach and a few other exceptions, there was little difference between the performances of the weighting schemes.

Residuals and error—The results reported previously in this section are useful to compare the performance of the *f* parameterization and the band-weighting schemes. However, it would be more useful to develop relationships that indicate the accuracy and precisions of individual inversions made with the same algorithm parameters. Given that the levels of environmental, atmospheric, and SIOP noise in an image and IOP set are essentially unknowable, it is not possible to determine an absolute value for the expected error. But, it should be possible to attach a relative reliability factor to the water quality constituent values retrieved from an image pixel.

The least squares technique finds the preferred solution by minimizing the residuals; therefore it is reasonable to presume that the sum of these residuals may be related to the adequacy of the solution. Scatter plots of the residual sum against the absolute value of the water quality constituent error for the MER_REF1 weighting scheme are shown in Fig. 11.

There is a clear linear trend shown in the scatter plots for the TSM and CDOM error for all weighting schemes. Lines of best fit applied to these have R^2 values ranging from 0.898 to 0.935 for TSM and 0.770 to 0.854 for CDOM. None of the weighting schemes showed any discernable trends between the Chl *a* retrieval error and the sum of the residuals.

Advantages and limitations—The method described in this paper provides a convenient simplification to allow for the complexity of the photon direction distribution in natural waters, rather than shedding any light onto the physics of the problem. The simulation demonstrates that significant improvements in the accuracy and precision of retrieved water quality constituent values can be obtained by using semianalytically estimated values for the proportionality value that are calculated for each band separately. Simulations were used to negate the unquantifiable errors associated with spatial and temporal patterns in the dynamic nature of the aquatic environment, which make it difficult to establish the retrieval accuracy for the water quality constituent concentrations. Therefore, the necessary caveat to attach to this result is that the calculated values will not translate directly to real world problems. It has been shown that the accuracy and precision of the exact solution is more susceptible to the $NE\Delta R(0^-)_E$. The noise effect may be reduced if the assumption that the noise in each band is independent is not valid.

Whereas the calculation of the absolute accuracy of any given water quality constituent retrieval is problematic, it has been shown that there is potential to at least assess its relative accuracy with respect to other pixels in the same image. The result presented above is a starting point to examine other methods that may involve properties such as the covariance of the water quality constituent retrievals.

The water quality constituent retrieval is sensitive to the value of the proportionality factor. We have allowed *f* to vary with respect to wavelength, IOP set, and sun position. It has been shown that *f* also varies with respect to the view zenith angle (Morel and Gentili 1993). No allowance has been made for this effect. Calculations based on Lee et al. (2004) showed that for a view zenith angle of 20°, the effect was of much less importance than the effect of the sun zenith angle.

Lastly, the paper shows that overdetermined systems can be used to mitigate the effect of unknown and endemic sources of error in the remote sensing system. However, the primary advantage is in ensuring a large number of bands are used rather than minor variations of relative weights that are assigned to each band. It was shown that the residuals left after the inversion can be used to assign reliability measures to the retrievals of TSM and CDOM but not for Chl *a*.

Comments and recommendations

It would be reasonable to assume that the functions derived for the proportionality factor will be dependent on the specific

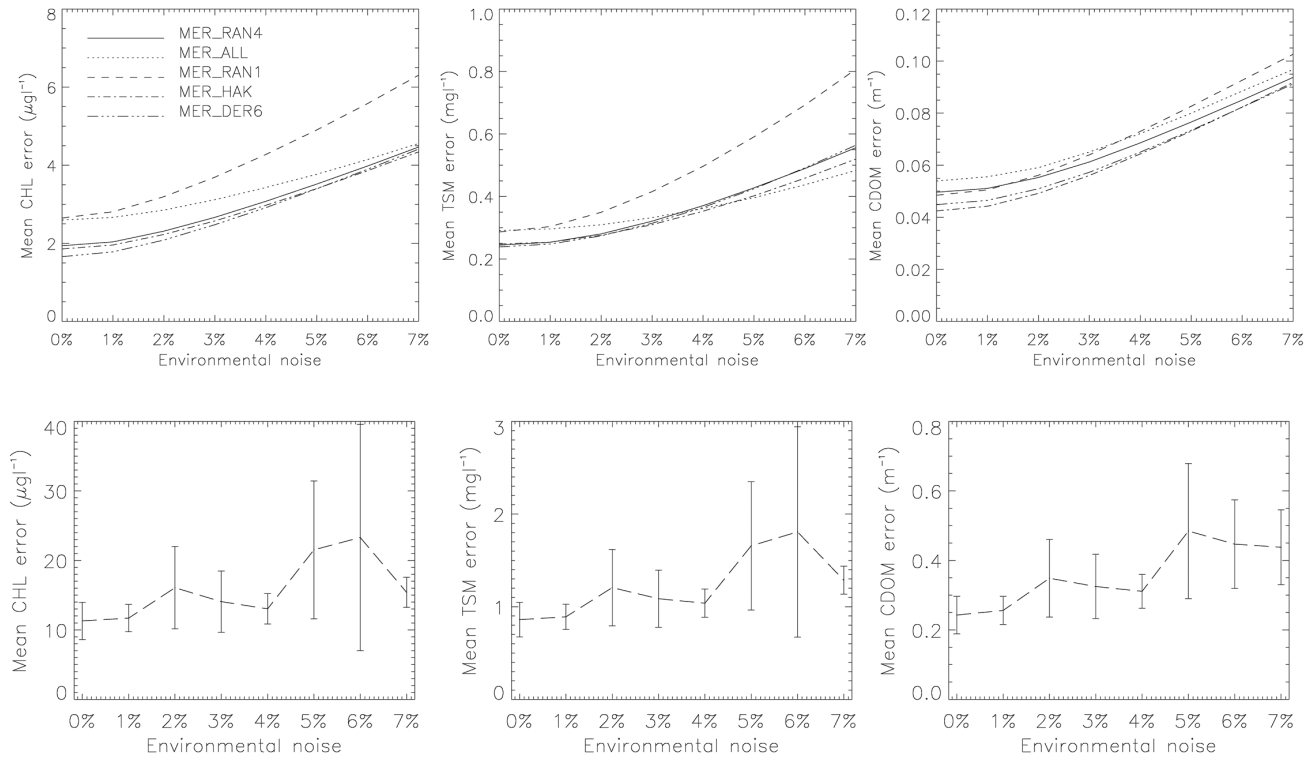

Fig. 7. Plot of the average error of water quality constituent retrieval against the environmental noise level for selected weighting schemes. MER_3BANDS has been plotted separately for clarity and is shown with its 95% confidence intervals.

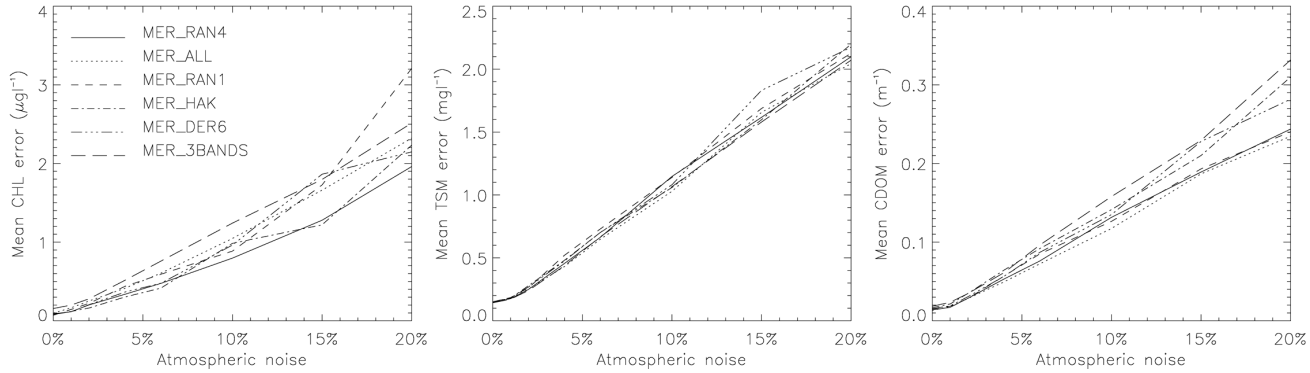

Fig. 8. Plot of the average error of water quality constituent retrieval against the atmospheric correction noise level for selected weighting schemes.

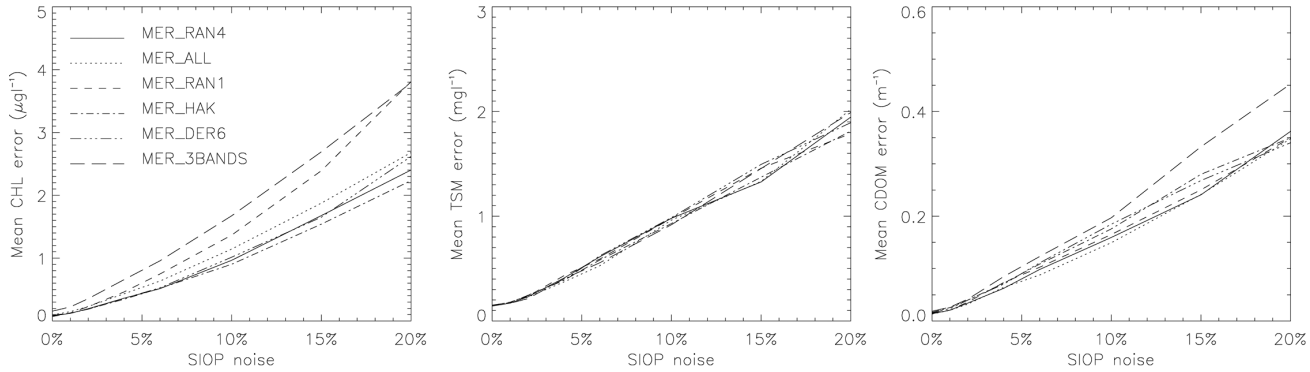

Fig. 9. Plot of the average error of water quality constituent retrieval against the SIOP noise level for selected weighting schemes.

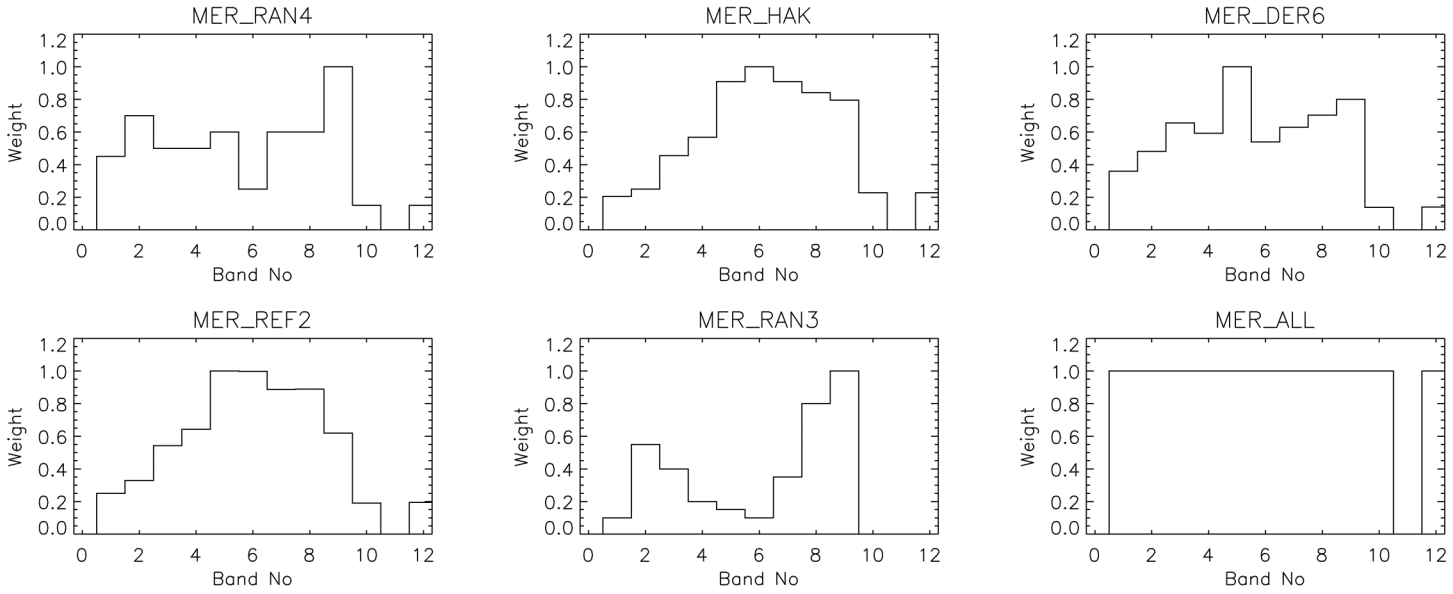

Fig. 10. Plot showing the weights for the six best performed weighting schemes. The schemes are shown in rank order from the best performed in the top left hand corner and the sixth best performed in the bottom right.

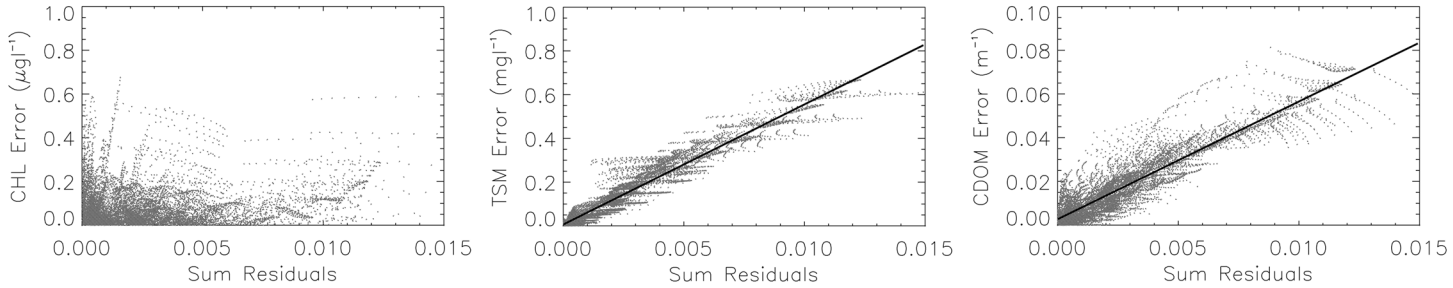

Fig. 11. Scatter plot of the residual sum against the absolute value of the water quality constituent error for the MER_HAK weighting scheme. Lines of best fit have been fitted to the TSM and CDOM plots with R^2 values of 0.916 and 0.846, respectively.

absorption and scattering values of the water quality constituents. If this is the case then a substantial pre-processing overhead will be required for application of the approach to each new water body. To confirm this assumption, the process described in this paper will need to be applied to larger multi-site in situ data sets of optical properties. As the nature of the proportionality factor variation was unknown, the selection of nine sun angles was made to ensure that there was less risk of overfitting data. In future, it should be possible to use fewer degrees of freedom and still obtain a reliable result. This would reduce the pre-processing overhead.

The article shows that there is no single band weighting scheme that is optimal for the retrieval of water quality constituents for Wivenhoe Dam. The selection of the weighting scheme will be dependent on which water quality constituent is the focus of the study or on the level of confidence the researcher has in the accuracy of various parameters and image corrections that contribute to the inversion. Clearly, the selection of the weighting scheme cannot be made without reference to the characteristics of the environment in which it is being employed.

The utility of the residual error relationship will be dependent on the heterogeneity of the water quality constituent horizontal distributions in the water body. If there is a limited range in the water quality constituent residual values then variability in the observed relationship will overwhelm the information from the relationship. If this is not the case, then water quality constituent retrieval reliability layers could be produced for the water quality constituent concentration maps. This would allow researchers or managers to decide whether the patterns observed in the water bodies were valid or merely artifacts from the uncertainty in the water quality constituent values.

References

Aas, E. 1987. Two-stream irradiance model for deep waters. Appl. Opt. 26:2095-2101.

Baruah, P. J., M. Tamura, K. Oki, and H. Nishimura. 2001. Neu-

ral network modeling of lake surface chlorophyll and suspended sediment from Landsat TM imagery. *In* Proceedings of 22nd Asian Conference of Remote Sensing. Centre for Remote Imaging, Sensing and Processing, National University of Singapore; Singapore Institute of Surveyors and Valuers, Asian Association on Remote Sensing. p. 911-916.

Boss, E., and C. S. Roesler. 2006. Over constrained linear matrix inversion with statistical selection. *In* Z. Lee [ed.], Remote sensing of inherent optical properties: Fundamentals, tests of algorithms, and applications. International Ocean-Colour Coordinating Group [IOCCG]. IOCCG report nr 5. p. 57-62. <http://www.ioccg.org/reports/report5.pdf>.

Brando, V. E., and A. G. Dekker. 2003. Satellite hyperspectral remote sensing for estimating estuarine and coastal water quality. IEEE T. Geosci. Remote 41:1378-1387.

Buiteveld, H., J. H. M. Hakvoort, and M. Donze. 1994. Optical properties of pure water, p. 174-183. *In* J. S. Jaffe [ed.], Proceedings of SPIE ocean optics XII. Proceedings/SPIE—the International Society for Optical Engineering.

Campbell, G., and S. R. Phinn. 2008. The efficacy of band weighting schemes for improving the accuracy and precision of water quality parameters estimated from MERIS and MODIS image data. *In* Proceedings of 14th Australasian Remote Sensing & Photogrammetry Conference. Spatial Sciences Institute. p. 12.

Clementson, L. A., J. S. Parslow, A. R. Turnbull, D. C. McKenzie, and C. E. Rathbone. 2001. Optical properties of waters in the Australasian sector of the Southern Ocean. J. Geophys. Res. Oceans 106:31611-31625.

De Haan, J. F., and J. M. M. Kokke. 1996. Remote sensing algorithm development TOOLKIT I: Operationalisation of tools for atmospheric correction of remote sensing data of coastal and inland waters. Beleidscommissie Remote Sensing.

Dekker, A. G., H. J. Hoogenboom, L. M. Goddijn, and T. J. M. Malthus. 1997. The relation between inherent optical properties and reflectance spectra in turbid inland waters. Remote Sens. Rev. 15:59-74.

Giardino, C., V. E. Brando, A. G. Dekker, N. Strombeck, and G. Candiani. 2007. Assessment of water quality in Lake Garda (Italy) using Hyperion. Remote Sens. Environ. 109:183-195.

Gordon, H. R., O. B. Brown, and M. M. Jacobs. 1975. Computed relationships between the inherent and apparent optical properties of a flat homogeneous ocean. Appl. Opt. 14:417-427.

———, and others. 1988. A semianalytic radiance model of ocean color. J. Geophys. Res. 93:10909-10924.

Hakvoort, H., J. F. de Haan, R. R. W. Jordans, R. J. Vos, S. W. M. Peters, and M. Rijkeboer. 2002. Towards airborne remote sensing of water quality in The Netherlands—validation and error analysis. ISPRS J. Photogramm. 57:171-183.

Hoge, F. E., and P. E. Lyon. 1996. Satellite retrieval of inherent optical properties by linear matrix inversion of oceanic radiance models: An analysis of model and radiance measurement errors. J. Geophys. Res. 101:16631-16648.

———, C. W. Wright, P. E. Lyon, R. N. Swift, and J. K. Yungel. 1999. Satellite retrieval of the absorption coefficient of phytoplankton phycoerythrin pigment: Theory and feasibility status. Appl. Opt. 38:7431-7441.

Hoogenboom, H. J., A. G. Dekker, and I. A. Althuis. 1998a. Simulation of AVIRIS sensitivity for detecting chlorophyll over coastal and inland waters. Remote Sens. Environ. 65:333-340.

———, A. G. Dekker, and J. F. de Haan. 1998b. Retrieval of chlorophyll and suspended matter from imaging spectrometry data by matrix inversion. Can. J. Remote Sens. 24:144-152.

Keller, P. A. 2001. Comparison of two inversion techniques of a semi-analytical model for the determination of lake water constituents using imaging spectrometry data. Sci. Total Environ. 268:189-196.

Kishino, M., M. Takahashi, N. Okami, and S. Ichimura. 1985. Estimation of the spectral absorption coefficients of phytoplankton in the sea. Bull. Mar. Sci. 37:634-642.

Lee, Z. [ed.]. 2006. Remote sensing of inherent optical properties: Fundamentals, tests of algorithms, and applications. IOCCG. IOCCG report nr 5. <http://www.ioccg.org/reports/report5.pdf>.

———, K. L. Carder, C. D. Mobley, R. G. Steward, and J. S. Patch. 1999. Hyperspectral remote sensing for shallow waters. 2. Deriving bottom depths and water properties by optimization. Appl. Opt. 38:3831-3843.

———, and ———. 2002. Effect of spectral band numbers on the retrieval of water column and bottom properties from ocean color data. Appl. Opt. 41:2191-2201.

———, ———, and K. Du. 2004. Effects of molecular and particle scatterings on the model parameter for remote-sensing reflectance. Appl. Opt. 43:4957-4964.

Lyon, P. E., and F. E. Hoge. 2006. The linear matrix inversion algorithm. *In* Z. Lee [ed.], Remote sensing of inherent optical properties: Fundamentals, tests of algorithms, and applications. IOCCG. IOCCG report nr 5. p. 49-56. <http://www.ioccg.org/reports/report5.pdf>.

Maffione, R. A., and D. R. Dana. 1997. Instruments and methods for measuring the backward-scattering coefficient of ocean waters. Appl. Opt. 36:6057-6067.

Matarrese, R., M. T. Chiaradia, V. De Pasquale, and G. Pasquariello. 2004. Chlorophyll-a concentration measure in coastal waters using MERIS and MODIS data. *In* 2004 IEEE International Geoscience and Remote Sensing Symposium proceedings: science for society: exploring and managing a changing planet: 20 – 24 September 2004: Anchorage Alaska, v. 6. IEEE. p. 3639-3641.

Mobley, C. D., and L. Sundman. 2001. Hydrolight 4.2 Users' Guide. Sequoia Scientific.

———, and others. 2005. Interpretation of hyperspectral remote-sensing imagery by spectrum matching and look-up tables. Appl. Opt. 44:3576-3592.

Morel, A. 1974. Optical properties of pure water and pure seawater, p. 1-24. *In* N. G. Jerlov and E. Steeman Nielsen [eds.], Optical aspects of oceanography. Academic.

———, and B. Gentili. 1993. Diffuse reflectance of oceanic waters. 2. Bidirectional aspects. Appl. Opt. 32:6864-6872.

O'Reilly, J. E., and others. 1998. Ocean color chlorophyll algorithms for SeaWiFS. J. Geophys. Res. 103:24937-24953.

Orr, P. T., and P. M. Schneider. 2006. Toxic cyanobacteria risk assessment: Reservoir vulnerability and water use best practice. SEQ Water.

Phinn, S. R., and A. G. Dekker [eds.]. 2005. An integrated remote sensing approach for adaptive management of complex coastal waters: The Moreton Bay case study. Cooperative Research Centre for Coastal Zone, Estuary & Waterway Management. Technical report no. 23. Further title page information: Final report - Moreton Bay remote sensing tasks (MR2): October 2004.

Pope, R. M., and E. S. Fry. 1997. Absorption spectrum (380–700 nm) of pure water. II. Integrating cavity measurements. Appl. Opt. 36:8710-8723.

Rijkeboer, M., A. G. Dekker, and H. J. Gons. 1997. Subsurface irradiance reflectance spectra of inland waters differing in morphometry and hydrology. Aquat. Ecol. 31:313-323.

Schaale, M., J. Fischer, and C. Olbert. 1998. Quantitative estimation of substances contained in inland water from multispectral airborne measurements by neural networks. *In* Proceedings of ASPRS-RTI Annual Conference. American Society for Photogrammetry and Remote Sensing. p. 1345-1356.

Schiller, H., and R. Doerffer. 1999. Neural network for emulation of an inverse model operational derivation of Case II water properties from MERIS data. Int. J. Remote Sens. 20:1735-1746.

Smith, R. C., and K. S. Baker. 1981. Optical properties of the clearest natural waters (200-800 nm). Appl. Opt. 20:177-184.

Stavn, R. H., and A. D. Weidemann. 1989. Shape factors, two-flow models, and the problem of irradiance inversion in estimating optical parameters. Limnol. Oceanogr. 34:1426-1441.

Su, F. C., C. R. Ho, Q. Zheng, N. J. Kuo, and C. T. Chen. 2006. Satellite chlorophyll retrievals with a bipartite artificial neural network model. Int. J. Remote Sens. 27:1563-1579.

Van Heukelem, L., and C. S. Thomas. 2001. Computer-assisted high-performance liquid chromatography method development with applications to the isolation and analysis of phytoplankton pigments. J. Chromat. A 910:31-49.

Vos, R. J., J. H. M. Hakvoort, R. R. W. Jordans, and B. W. Ibelings. 2003. Multiplatform optical monitoring of eutrophication in temporally and spatially variable lakes. Sci. Total Environ. 312:221-243.

Walker, R. E. 1994. Marine light field statistics. Wiley.

WET Labs. 2005. ac-9 Protocol document. Revision J, 11 April 2005.

Submitted 6 April 2009
Revised 10 November 2009
Accepted 12 November 2009